Nanoscale

Accepted Manuscript

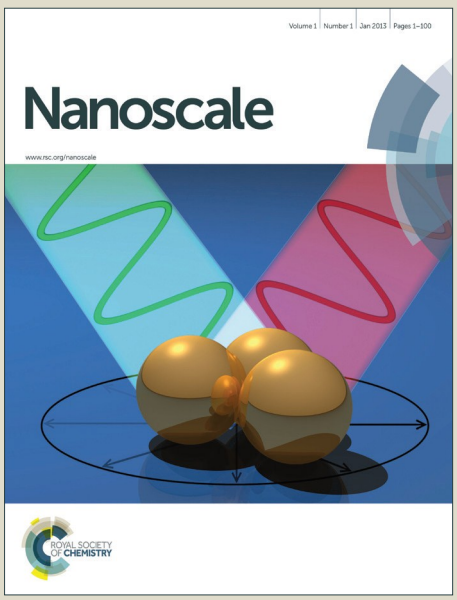

ROYAL SOCIETY OF CHEMISTRY

www.rsc.org/nanoscale

Journal Name

ARTICLE

Melamine-Assisted One-Pot Synthesis of Hierarchical Nitrogen-Doped Carbon@MoS_2 Nanowall Core-Shell Microspheres and Their Enhanced Li-Storage Performances

Received 00th January 20xx,
Accepted 00th January 20xx

DOI: 10.1039/x0xx00000x

www.rsc.org/

Fugen Sun,[a] Yanju Wei,[b] Jianzhuang Chen,[a] Donghui Long,*[b] Licheng Ling,[b] Yongsheng Li[a] and Jianlin Shi*[a,c]

A facile and scalable one-pot approach has been developed to synthesize carbon@MoS_2 core-shell microspheres by a hydrothermal method, which involves the fast formation of melamine-resorcinol-formaldehyde polymeric microspheres *in situ*, and followed by directly growth of the MoS_2 nanowalls on them. The results give unequivocal proof that the melamine could be the key to forming the core-shell microspherical morphology, and the contents of MoS_2 shells can be easily tuned by initial ratios of the precursors. After simple heat treatment, the obtained carbon@MoS_2 microspheres simultaneously integrate the nitrogen-doped carbon cores and the hierarchical shells which consist of few-layered MoS_2 nanowalls with an expanded interlayer spacing. There unique architectures are favourable for high electronic/ionic conductivity and accommodate volume strain during the electrochemical reaction of the MoS_2 anodes in lithium-ion batteries. Thus, a very high reversibility capacity of 771 mAh g^{-1} at 100 mA g^{-1} after 100 cycles, and rate capacity of 598 mAh g^{-1} at 2000 mA g^{-1} could be achieved for the carbon@MoS_2 core-shell microspheres with the optimal composition. Furthermore, a thin carbon coating on the carbon@MoS_2 microspheres could further increase the reversible capacity to 856 mAh g^{-1} after 100 cycles at 100 mA g^{-1}. These encouraging results suggesting that such a facile and efficient protocol can provide a new pathway to produce hierarchical core-shell microspheres which integrate the structural, morphological and compositional design rationales for advanced lithium-ion batteries.

Introduction

Lithium-ion batteries are considered to be a promising energy-storage solution for ever-increasing energy demands and environmental concerns. However, the currently commercial graphite anode cannot fully meet the higher energy/power density requirements due to its relatively low capacity (372 mAh g^{-1}).[1,2] Molybdenum disulfide (MoS_2), as a typical layered transition metal sulfide, has an analogous structure to graphite and a significantly larger interlayer distance of ca. 0.6 nm,[3,4] which allows a fast diffusion path for movement of lithium ions.[5,6] Moreover, MoS_2 theoretically incorporates with 4 mol Li through the conversion reaction, accounting for 670 mAh g^{-1} Li storage capacity that is much higher than that of the graphite electrode.[7,8] It is not, therefore, surprising that the MoS_2 anode attracts considerable attention of battery developers. However, there are some inherent problems for the MoS_2 anode hampering its final application: (1) poor cycle stability due to the severe structure collapse caused by the large volume change during charge-discharge cycles;[9] (2) low columbic efficiency due to the formation of solid electrolyte interface film from electrolyte degradation;[10] and (3) low utilization and limited rate capacity due to the poor electronic conductivity of MoS_2.[11]

In order to overcome the above problems, several technological contributions are attempted.[12,13] Improvements can be achieved through compositing MoS_2 with the conductive carbonaceous materials, such as amorphous carbons,[14,15] carbon nanotubes,[16,17] ordered mesoporous carbons[18] or graphene.[19,20] In this way, the conductive carbon framework provides the elastic support and generates essential electrical contact to MoS_2.[21] Meanwhile, the carbon phase acts as a protective layer and then reduces the electrolyte degradation.[22,23] As a result, the effective utilization of MoS_2 and the cycling stability are certainly improved. Another effective approach to improve the reversible capacity is making MoS_2 materials into the nanometre scale such as nanospheres,[24] nanorods,[25] nanotubes[26] and nanosheets,[27] due to their large surface areas, the short distances and the enhanced electrochemical kinetics.

[a] *Lab of Low-Dimensional Materials Chemistry, School of Materials Science and Engineering, East China University of Science and Technology, Shanghai 200237, China. Fax: +86-21-52412712; Tel: +86-21-52412722; E-mail: jlshi@mail.sic.ac.cn*
[b] *State Key Laboratory of Chemical Engineering, East China University of Science and Technology, Shanghai 200237, China. Fax: +86-21-64252914; Tel: +86-21-64252914; E-mail: longdh@mail.ecust.edu.cn*
[c] *State Key Laboratory of High Performance Ceramics and Superfine Microstructure, Shanghai Institute of Ceramics, Chinese Academy of Sciences, Shanghai 200050, China*
† Electronic Supplementary Information (ESI) available. See DOI: 10.1039/x0xx00000x

Furthermore, constructing hierarchical three-dimensional architectures on the basis of MoS_2 nanoscaled building blocks could further achieve the good stability.[28] Such architectures synergistically enhance the features of both nanomaterials and micromaterials, and provide the sufficient void spaces between the nanosheets which effectively buffer the mechanical stress and volume variation during the charge-discharge cycles.[29] Besides the morphologies, the enlarged interlayer distance of Mo-S-Mo is critically important to facilitate Li-ion diffusion in the solid state phase of MoS_2 materials.[30] However, one of these design strategies alone leads to only limited improvement in cyclability of MoS_2-based anode materials. A systematic material design strategy is intended to promote the electrochemical performances.

In this respect, the core-shell structures are endowed with the advantages to combine varied design rationales together, and therefore should be an integrated and effective strategy to obtain the high Li storage performances for MoS_2 electrode materials.[31] In general, the core-shell structures are prepared *via* the "post-synthesis" approaches, where the core particles are firstly synthesized and separately incorporated into the systems with proper surface modifications for coating the shell materials.[32, 33] However, it is inevitable that this method commonly requires multi-step and energy-consuming processes. By contrast, "couple synthesis" in the one-pot process represents an attractive strategy for the preparation of the core-shell structures, which takes advantage of the reaction sequences and thus exhibits higher efficiency and facility.[34, 35] However, up to now, this method has not been as well developed as the "post-synthesis" methods, and its controlled synthesis of the well-defined core-shell structure with distinctive nano/micro-scaled morphology is still a great challenge. Therefore, this puts forward higher challenges for developing a facile and scalable approach to controllably synthesize the advanced core-shell-structured MoS_2 materials with a systematic material design strategy for the Li-storage application.

Herein, we developed a facile one-pot, melamine-assisted hydrothermal method to controllably synthesize hierarchical carbon@MoS_2 core-shell microspheres by the "couple synthesis" approach, which involves the fast formation of melamine-resorcinol-formaldehyde polymeric microspheres *in situ*, and followed by directly growth of the MoS_2 nanowalls on them. The melamine could be the key to forming the core-shell microspherical morphology, and the contents of MoS_2 shells can be easily tuned by initial ratios of the precursors. After simple heat treatment, the obtained carbon@MoS_2 microspheres consist of the nitrogen-doped carbon cores and the hierarchical shells based on few-layered MoS_2 nanowalls with an expanded interlayer spacing. These unique architectures simultaneously integrate the structural, morphological and compositional design rationales, thus possessing the excellent structural stability and transport advantages for both electrons and Li-ions. The hierarchical carbon@MoS_2 core-shell microspheres exhibit a high reversibility capacity of 771 mAh g^{-1} with a columbic efficiency of 97.7 % at 100 mA g^{-1} after 100 cycle, and rate capacity of 598 mAh g^{-1} at 2000 mA g^{-1}. Furthermore, we coated a thin carbon skin on the carbon@MoS_2 core-shell microspheres to further improve the electrode performances. With the assistance of carbon coating, considerable enhancement in the cycle stability was achieved. These encouraging results suggest that such a facile and efficient protocol can provide a new pathway to produce core-shell microspheres on the basis of hierarchical nanoarchitectures for advanced lithium-ion batteries.

Experimental Section

Preparation of nitrogen-doped carbon@MoS_2 (NC@MoS_2) core-shell microspheres

The nitrogen-doped carbon@MoS_2 (NC@MoS_2) core-shell microspheres were synthesized via a facile one-pot hydrothermal method and subsequent heat-treatment. Melamine (M), resorcinol (R) and formaldehyde (F) were used as the carbon precursors, and Na_2MoO_4 and NH_2CSNH_2 were used as the MoS_2 precursors. In a typical synthetic procedure, 0.88 g resorcinol (8 mmol) and 1.29 g formaldehyde (37 wt. %, 16 mmol) were dissolved in 30 ml distilled water and then stirred at 40 ^oC for more than 1 h. Subsequently, 1.01 g melamine (8 mmol) and 1.94 g formaldehyde (37 wt. %, 24 mmol) were dissolved in 30 ml distilled water at 80 ^oC with consecutive agitation until the solution became clear. The above MF solution was cooled down to 40 ^oC and then added into the RF solution with continually stirred for 30 min. 2.40 g Na_2MoO_4 and 4.80 g NH_2CSNH_2 were dissolved in the above MRF mixed solution, and was then transferred to a 100 ml Teflon lined autoclave (70 % filling) and heated at 180 ^oC for 24 h under a static condition. The precipitates were recovered by filtration, washed with distilled water and air dried at 100 ^oC. The resultant NC@MoS_2 core-shell microspheres were obtained by carbonizing the precipitates at 800 ^oC for 3h in nitrogen flow with a heating rate of 5 ^oC min^{-1}. In this work, by the control of the weight ratios of Na_2MoO_4 to the melamine-resorcinol-formaldehyde (MRF) precursor in the initial hydrothermal solution, four samples of NC@MoS_2 core-shell microspheres with different MoS_2 contents were prepared, which were denoted as NC@xMS, where x wt.% represents the weight content of MoS_2 in the NC@MoS_2 core-shell microspheres.

Preparation of carbon-coated NC@MoS_2 microspheres

The carbon-coated NC@MoS_2 microspheres were synthesized by carbon coating the above uncarbonized MRF@MoS_2 core-shell microspheres using glucose through in-situ hydrothermal polymerization and carbonization. Typically, 5.0 g MRF@MoS_2 core-shell microspheres were re-dispersed in a 70 ml solution containing 1.0 g glucose, and then placed into a 100 ml Teflon lined autoclave and heated at 180 ^oC for 12 h under a static condition. The resulting carbon-coated NC@MoS_2 microspheres were obtained by filtration, drying at 100 ^oC and carbonization at 800 ^oC for 3 h in N_2 flow.

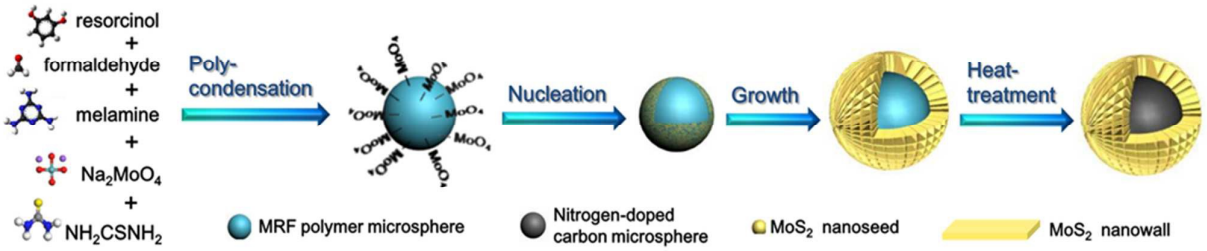

Fig. 1. Schematic representation of the formation process of the hierarchical NC@MoS_2 core-shell microspheres.

Materials Characterization

The thermogravimetric analysis (TGA Instrument Q600 Analyser) was carried out at an air flow rate of 100 ml min^{-1}. The samples were heated to 700 ^oC with a rate of 10 ^oC min^{-1}. The X-ray diffraction (XRD) patterns were acquired on a Rigaku D/max 2550 diffractometer operating at 40 KV and 20 mA using Cu Kα radiation (λ = 1.5406 Å). The Raman spectra was recorded with a Renishaw system 1000 with an argon-ion laser operating at 514 nm with a charged-coupling-device detector. The morphologies of samples were observed under scanning electron microscopy (SEM, JEOL 7100F) and transmission electron microscopy (TEM, JEOL 2100F). The energy dispersive X-ray spectroscopy (EDX) analysis were performed under scanning electron microscopy (SEM, FEI Q-300). The zeta potential of the colloidal microsphere was conducted using a Malvern Zetasizer Nano-ZS90 DLS system equipped with a He-Ne laser at a wave length of 632.8 nm. Nitrogen adsorption-desorption isotherms were measured at 77 K with a Quadrasorb SI analyser. Before the measurements, the samples were degassed under vacuum at 473 K for 12 h. The Brunauer-Emmett-Teller (BET) method was utilized to calculate the specific surface areas. The total pore volume V_t was calculated using a single point at relative pressure of 0.985. The pore size distributions were derived from desorption branch by using the Barrett-Joyner-Halenda (BJH) model.

Electrochemical measurements

The carbon-MoS_2 composite anodes were slurry-cast onto Cu current collectors. Typically, 80 wt.% of the carbon-MoS_2 composite, 10 wt. % carbon black (Super P Conductive Carbon Black) and 10 wt. % PVDF were mixed with N-methyl-2-pyrrolidone (NMP). The slurries were coated on Cu current collectors and dried at 100 ^oC overnight. Electrochemical tests of these electrode materials were performed using coin cells with the carbon-MoS_2 composite cathodes and lithium metal as the counter electrodes. The average weight of the working electrodes was approximately 2 mg and the diameter was 11 mm.The electrolyte was 1 M $LiPF_6$ dissolved in EC/DMC/DEC (1:1:1 by volume) and the separator was a microporous membrane (Celgard 2400). The cell was assembled in an argon filled glove box. The galvanostatic charge-discharge test and cyclic voltammetry measurements (CV) were conducted using an Arbin battery cycler (Arbin, BT2000, USA). All capacity values were calculated on the basis of total carbon-MoS_2 composite mass. Electrochemical impedance spectroscopy (EIS) was performed with an electrochemical working station PCI4/300 (Gamry Instrument, Warminster, PA, USA). The sinusoidal excitation voltage applied to the coin cells was 5 mV, with frequency range from 100 kHz to 0.01 Hz. All the electrochemical tests were performed at room temperature.

Results and discussion

The facile one-pot synthetic protocol for the nitrogen-doped carbon@MoS_2 (NC@MoS_2) core-shell microspheres is illustrated in Fig. 1. The carbon precursors including melamine (M), resorcinol (R) and formaldehyde (F), the molybdenum precursor (Na_2MoO_4) and the sulfur source (NH_2CSNH_2) were mixed together in an autoclave, followed by a hydrothermal process at 180 ^oC and subsequent heat-treatment in N_2 flow at 800 ^oC. The coverage of MoS_2 on the carbonaceous microspheres is accomplished by the "couple synthesis" approach which takes advantage of the formation sequences between cores and shells: the fast formation of the carbonaceous microspheres, and subsequent nucleation and growth of the MoS_2 nanowalls.

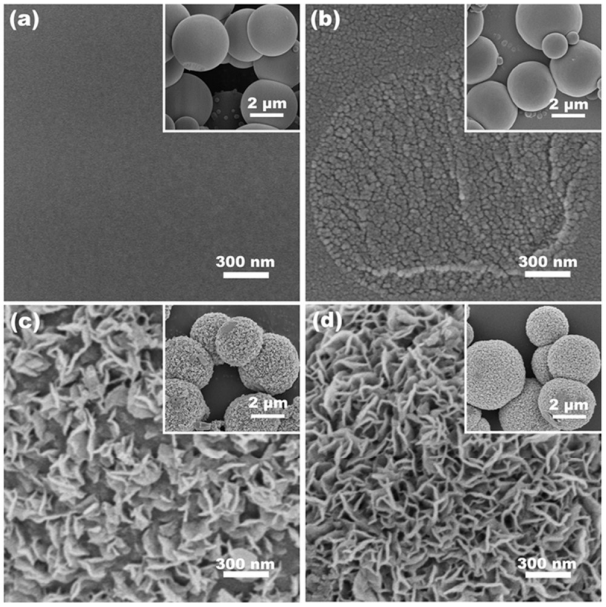

Fig. 2. Typical SEM images of the surfaces of as-synthesized MRF@MoS_2 microspheres at different hydrothermal times without heat-treatment: (a) 1 h, (b) 2 h, (c) 6 h and (d) 24 h. Insets in (a-d) are the low-magnification SEM images of their overall morphologies, respectively.

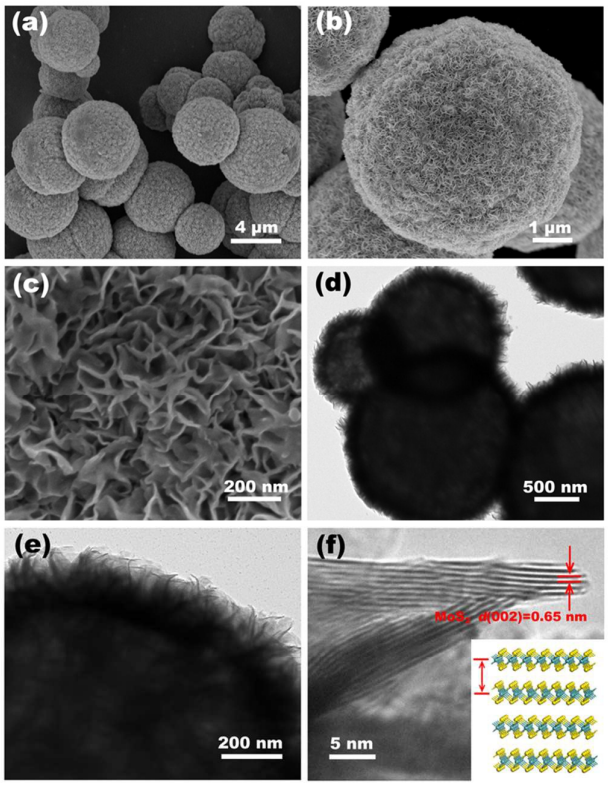

Fig. 3. SEM images of the NC@70MS core-shell microspheres: (a) the overall morphologies, (b) the single microsphere and (c) the shell surface of the microspheres; TEM images of the NC@70MS core-shell microspheres: (d) the overall morphologies and (e) the magnified edge part of the single microsphere; (f) HRTEM image of the MoS_2 nanowalls of the NC@70MS core-shell microspheres. Inset in (f) is the schematic model of hexagonal 2H-MoS_2 phase.

The formation process of these core-shell microspheres could be visually confirmed by the time-dependent experiments where other experimental conditions such as the hydrothermal temperature and reactants concentration are kept the same. At the initial hydrothermal time of 1 h, the collected samples are MRF polymer microspheres with smooth surfaces (Fig. 2a) and contain almost no MoS_2 determined from TGA analysis in air (Fig. S1). After hydrothermal reaction for 2 h, the MRF microsphere surfaces are covered by MoS_2 nuclei nanoparticles with a content of 3.2 wt.% (Fig. 2b and Fig. S1). With the hydrothermal time to 6 h, small amounts of MoS_2 nanowalls have grown and spread sporadically on the MRF microsphere surfaces (Fig. 2c). Finally, these nanowalls could fully cover the MRF microspheres and become dense to form a net-like array with a prolonged reaction time of 24 h (Fig. 1e). The increasement of MoS_2 contents in the TG results (Fig. S1) and the presence of hexagonal 2H-MoS_2 phase in the XRD patterns of MRF@MoS_2 composites (Fig. S2) as the hydrothermal reaction progress further suggest the continuous growth of MoS_2 nanowalls on the fast formed MRF polymer microspheres. Moreover, without the addition of melamine in the initial hydrothermal precusors, the as-prepared RF/MoS_2 composites show irregular morphology (Fig. S3). Given that the basic malamine could accelerate the polymerization of resorcinol and formaldehyde as described in our previous work,[36] it leads to the fast formation of MRF microspheres, thus facilitating the consequent step of *in situ* growth of MoS_2 nanowalls in time. In addition, the increased surface charge of MRF microsphere caused by nitrogen functionality (Fig. S4) is favorable for the adsorbtion of MoO_4^{2-} anion and subsequent coating of MoS_2, which could further inhibit the continuous growth of MRF microspheres. Therefore, it is evident that the melamine could be the key to forming the core-shell microspherical morphology.

After simple heat-treatment, the MRF polymer is carbonized into conductive nitrogen-doped carbon while the hierarchical core-shell microspherical structures are perfectly preserved, as shown in Fig. 3. The MoS_2 content in the NC@MoS_2 microspheres is 71.4 wt.%, which designated as NC@70MS. The NC@MoS_2 microspheres exhibit a diameter size of about 1-7 μm. The TEM image in Fig. 3d and elemental EDX results in Fig. S5 reveal the nitrogen-doped carbon cores are in the middle site of the microspheres due to the conformal coverage of the MoS_2 shells. The SEM image in Fig. 3c and TEM image in Fig. 3e show the MoS_2 shell have an open-outside network structure which is build out of the inter-connected ultrathin nanowalls. The open space between nanowalls is relatively large. Such hierarchical porous structures could not only facilitate the diffusion of Li-ion, but also accommodate the large volume expansion during the charge-discharge cycles. The high-resolution TEM image in Fig. 3f clearly shows that the nanowalls display a perfect layered crystal with an (002) interlayer distance of 0.65 nm. Each MoS_2 nanowall is composed of 6-10 layers bonded together by van der waals interactions. Such few-layered nanowalls with an enlarged interlayer distance should be favourable for the fast lithium diffusion and high lithium storage.

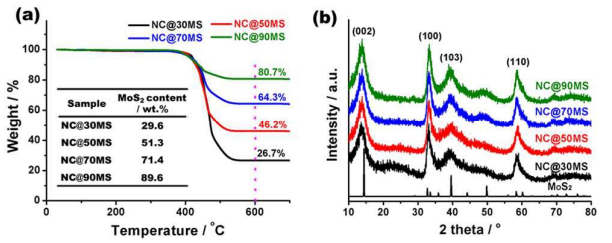

Fig. 4. (a) TGA analysis in air and (b) XRD patterns of the NC@MoS_2 core-shell microspheres with different MoS_2 contents; Inset in (a) lists the MoS_2 contents in the NC@MoS_2 microspheres determined from the remaining mass of pure MoO_3 in TGA results in air.

The contents of MoS_2 in the NC@MoS_2 microspheres could be easily tuned by changing the weight ratios of Na_2MoO_4 to the MRF precursors in the initial hydrothermal solution. To facilitate the evaluation of the electrochemical performances, except for the NC@70MS microspheres, here we prepared other three samples of the NC@MoS_2 microspheres (respectively denoted as NC@30MS, NC@50MS, and NC@90MS) in which the MoS_2 contents were designed to 30 wt.%, 50 wt.% and 90 wt.%. Furthermore, the MoS_2 content of each sample was confirmed using TG analysis (Fig. 4a), which was in good agreement with the designed composition. The Raman spectra of the NC@MoS_2 microspheres (Fig. S6) shows the typical characteristic E_{2g} and A_{1g} bands of MoS_2, respectively located at ca. 380.7 and 406.5 cm^{-1}. The XRD characterization (Fig. 4b) indicates that the MoS_2 in all these samples exhibit standard hexagonal 2H-MoS_2 phase. Furthermore, All the MoS_2 possess the same (002) interlayer distance of ca. 0.64 nm calculated from the Bragg's equation. No obvious diffraction peaks for carbon are observed, due to the shield effect of MoS_2 phase on the amorphous carbon.

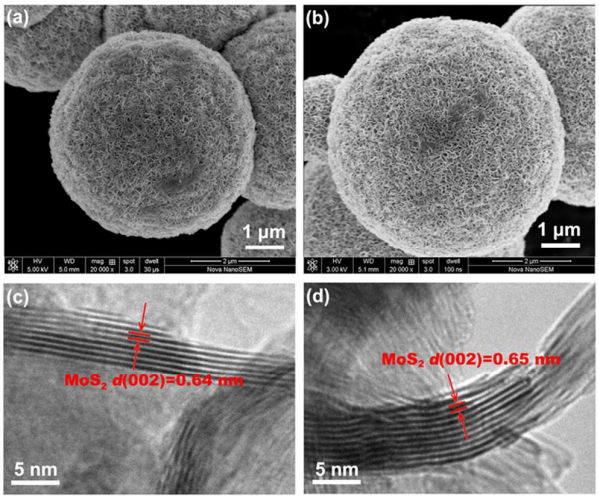

Fig. 5. SEM images of (a) the NC@30MS and (b) the NC@90MS core-shell microspheres; HRTEM images of the MoS_2 nanowalls of (c) the NC@30MS and (d) the NC@90MS core-shell microspheres.

The SEM and HRTEM images of the NC@MoS_2 microspheres with different MoS_2 contents are shown in Fig. 5, Fig. 3 and Fig. S7. All these NC@MoS_2 core-shell microspheres have the hierarchical MoS_2 shells constituted of few-layered MoS_2 nanowalls with a similar interlayer spacing. The similar porous structures are also shown in Fig. S7 and Table S1. The similar morphology and tunable components of the carbon@MoS_2 microspheres indicate the significance of our synthetic method for designing electrode materials with optimal performances.

To demonstrate the integrated structural and compositional design rationales of the hierarchical NC@MoS_2 core-shell microspheres, the electrochemical performances of all the samples were evaluated by cyclic voltammetry (CV),

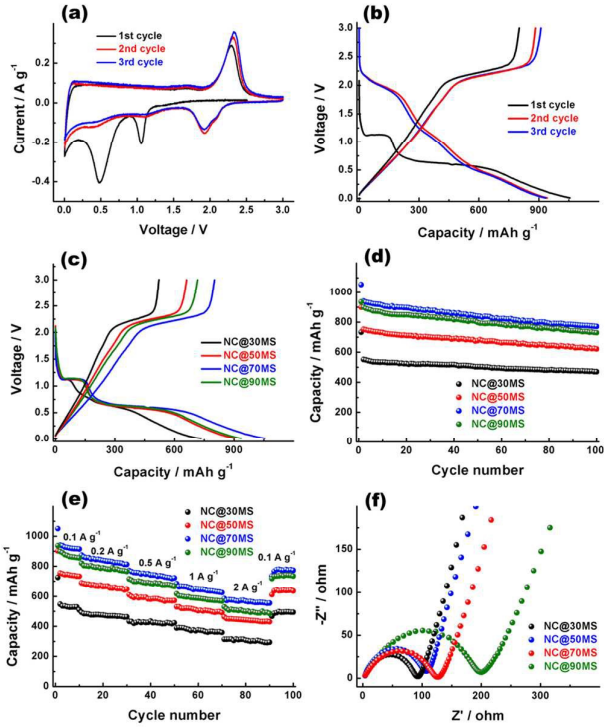

Fig. 6. (a) Cyclic voltammograms at 0.2 mV s^{-1} and (b) discharge-charge curves at 100 mAh g^{-1} of the NC@70MS core-shell microspheres; (c) initial discharge-charge curves at 100 mA g^{-1}, (b) cycle stability at 100 mA g^{-1}, (c) rate capacity and (d) EIS before the first cycle of the NC@MoS_2 core-shell microspheres with different MoS_2 contents.

galvanostatic charge-discharge testing, and electrochemical impedance spectroscopy (EIS). The CV curves of the NC@70MS core-shell microspheres scanned at 0.2 mV s^{-1} are shown in Fig. 6a. During the first cycle, two well-defined reduction peaks exist distinctly, which are centered at 1.06 V and 0.49 V corresponding to the Li insertion into the interlayer of MoS_2 and the conversion reaction of the lithium intercalates (Li_xMoS_2) to form metallic Mo and Li_2S, respectively.[37,38] The intense oxidation peak at 2.33 V could be attributed to the oxidation of Li_2S into sulfur.[39, 40] In the second and subsequent cycles, the pronounced reduction and oxidation peaks respectively centered at 1.92 V and 2.33 V are clearly observed, indicating that the lithiation/delithiation processes after the first cycle are dominated by the conversion between Li_2S and sulfur akin to Li-S batteries. The overlapped redox onset potential after the first cycle promises a good electrochemical reversibility of the NC@MoS_2 core-shell microspheres.

The discharge and charge profiles at a current rate of 100 mA g^{-1} of the NC@70MS core-shell microspheres are shown in Fig. 6b. Two plateaus, corresponding to the Li insertion into the interlayer of MoS_2 at 1.1 V and the conversion reaction of the lithium intercalates (Li_xMoS_2) to form metallic Mo and Li_2S at 0.6 V, are observed in the first discharge process, which agree well with two apparent reduction peaks in CV curves. In the

second and subsequent discharge sweeps, one slope plateau at ~ 2.0 V appears, which is related to the conversion reaction between Li_2S and sulfur. The initial discharge and charge capacities of the NC@70MS core-shell microspheres are 1054 and 801 mAh g^{-1} (All capacity values in this work were calculated on the basis of total carbon-MoS_2 composite mass), corresponding to a initial columbic efficiency of 76%. The irreversible capacity loss could be mainly attributed to the formation of solid electrolyte interface (SEI) film from the electrochemically driven electrolyte degradation, or the trapping of lithium inside the lattice.[41,42] The discharge and charge capacities in the second cycle are 941.6 and 883.2 mAh g^{-1}, respectively, giving rise to a coulombic efficiency of 93.8% and this value further increases to 97.5% in the third cycle, indicating very stable electrochemical reversibility after the first cycle.

The cycle stability of the NC@70MS core-shell microspheres at a current rate of 100 mA g^{-1} is shown in Fig. 6d. A high reversible capacity of 771 mAh g^{-1} with a columbic efficiency of 97.7 % (Fig. S9) is maintained after 100 cycles, suggesting the excellent structure stability upon cycles. Regardless of the contribution of carbon core (28.6 wt.%) to lithium storage capacity (Fig. S10), the MoS_2 shell can deliver much higher reversible capacities than the theoretical value (670 mAh g^{-1}) of MoS_2 based on the conventional conversion mechanisms. The obvious extra capacity could be attributed to that the newly-generated Mo^0 from MoS_2 during the discharge process could greatly activate and promote the reversible decomposition and formation of some SEI components, as reported in the literatures.[43, 44, 45] Fig. 6e shows the impressive rate capacity of the NC@70MS core-shell microspheres. Even at the maximum current rate of 2000 mA g^{-1}, the NC@70MS core-shell microspheres deliver 598 mAh g^{-1} after 70 cycles. The excellent stability of the NC@70MS core-shell microspheres is also evidenced by the recovery of a capacity of 773 mAh g^{-1} after 100 cycles when the current rate returns from 2000 mA g^{-1} to 100 mA g^{-1}. Such electrochemical performances are much higher than that of the hierarchical MoS_2 microspheres reported by Lou et al.[46] They reported that the hierarchical MoS_2 microspheres synthesized by the assistance of polystyrene, displayed the reversible capacity of 585 mAh g^{-1} after 100 cycles at a current rate of 100 mA g^{-1}. Yang et al. found that the hierarchical MoS_2/polyaniline nanowires prepared from the MoO_x-based organic-inorganic hybrid nanowires, exhibited the specific capacity of 320 mAh g^{-1} at 1000 mA g^{-1}.[47] The higher lithium storage capacity and cycling stability obtained in our work could be definitely ascribed to the unique hybrid hierarchical nanoarchitectures of the core-shell microspheres. First, the carbon cores provide robust supports to prevent the collapse of metastable MoS_2 shells and enhance the electronic conductivity of inter-connected MoS_2 nanowalls. Second, the hierarchical porous among the adjacent MoS_2 nanowalls in the shells could facilitate the electrolyte penetration and accommodate the large volume expansion during the charge-discharge cycles. Third, the ultrathin feature of the MoS_2 nanowalls could provide large electro-active surface area and short electronic/ionic transport path. In addition, the expanded interlayer distances of Mo-S-Mo could facilitate the fast Li-ion diffusion and improve the reaction reversibility. All these synergies result in the excellent structural stability and the fast electronic/ionic transportation, and in turn, high lithium storage capacities and stable cycling life are obtained.

The electrochemical performances of the NC@MoS_2 core-shell microspheres are strongly affected by the MoS_2 contents, as shown in Fig. 6c-f. Undoubtedly, significant decline in the specific capacity could be observed as decreasing the MoS_2 content from 70 wt.% to 30 wt.% due to the lower specific capacity of carbon compared with that of MoS_2 (Fig. 6c-e and Fig. S10). However, while the MoS_2 content is up to 90 wt.%, the NC@90MS microspheres exhibit a slightly lower MoS_2 utilization with a initial discharge capacity of 935 mAh g^{-1} and reversible capacity of 730 mAh g^{-1} after 100 cycles, lower than the values of the NC@70MS core-shell microspheres. This is possibly due to the significant deterioration of electronic/ionic conductivity caused by the excess MoS_2 coverage. This can be further confirmed by the EIS analysis (Fig. 6f). The semicircle diameters in the high frequency region of Nyquist plots indicate that the charge-transfer resistances are highest in the NC@90MS microspheres. These results further confirm the optimal components of the cores to shells are highly important to obtain the best electrochemical performances.

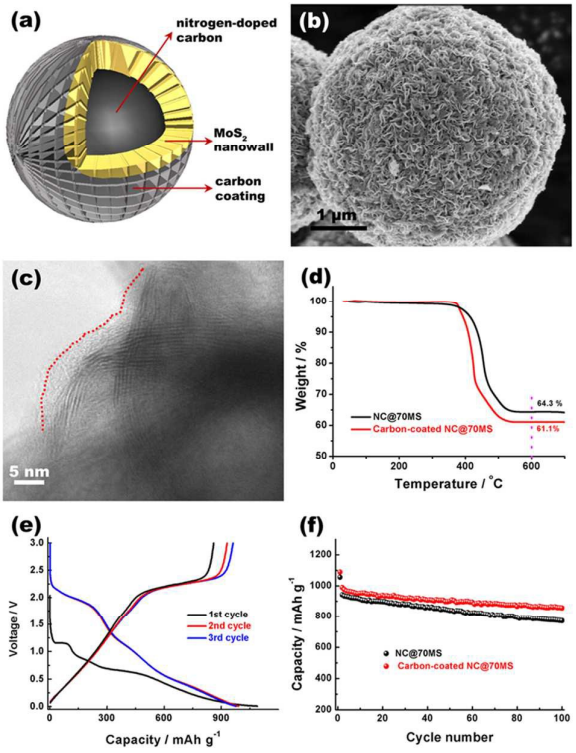

Fig. 7. Schematic model of the NC@MoS_2@C core-shell-shell sandwich microspherical structure (a). Characterizations of the carbon coated-NC@70MS microspheres: (b) SEM image, (c) TEM image of the MoS_2 nanowalls, (d) TG analysis in air, (e) initial discharge-charge curves and (f) cycle stability at 100 mA g^{-1}.

Evidently, the unique hierarchical NC@MoS_2 core-shell microspheres provide structural stability and electrons/ion transport advantages, synergistically maintaining the high lithium storage capacity and stable cycling life. However, a large irreversible capacity loss is still observed in the initial cycle as described above, mainly due to the formation of the thick solid electrolyte interface (SEI) film from electrolyte degradation. On the basis of the hierarchical NC@MoS_2 core-shell microspheres, here we further employed the carbon coating to inhibit the side reaction of active materials with the electrolyte and simultaneously enhance the electron conductivity.

The typical SEM image of the carbon coated-NC@70MS composites is shown in Fig. 7b. After carbon coating, the hierarchical microspherical structures are still completely retained. The HRTEM image in Fig. 7c gives a close-up view of 4-5 nm thick amorphous carbon layer evenly coating on the MoS_2 nanowalls, confirming the carbon coated-NC@MoS_2 microspherical structures (Fig. 7a). The TGA curves in air (Fig. 7d) suggest that the carbon coated-NC@70MS microspheres are composed of 27.2 wt.% nitrogen-doped carbon core, 67.9 wt.% MoS_2 shell and 4.9 wt.% carbon coating. When cycled at 100 mA g^{-1}, the carbon coated-NC@70MS microspheres exhibit a much higher initial columbic efficiency of 79% than the NC@70MS microspheres (Fig. 7e). With the assistance of carbon coating, a higher reversible capacity of 856 mAh g^{-1} is maintained after 100 cycles (Fig. 7f). Such high reversible capacity of the carbon coated-NC@70MS microspheres is among the highest values reported for the MoS_2 composite anodes.[16,17,25,26,32] The carbon coating is expected to enhancing the interface stability between the electrolyte and the MoS_2 electrode and promising the fast electron transfer (Fig. S11).

Conclusion

In conclusion, a facile one-pot hydrothermal method has been developed to construct carbon@MoS_2 core-shell microspheres using melamine, resorcinol and formaldehyde as the carbon precursors, Na_2MoO_4 as the molybdenum precursor and NH_2CSNH_2 as the sulfur source. The construction of the core-shell microspheres involves the fast formation of nitrogen-doped carbonaceous cores *in situ*, and followed by coating the MoS_2 shells through the growth of the nanowalls without additional surface treatment. The melamine could be the key to forming the core-shell microspherical morphology, possibly via accelerating the fast formation of carbonaceous microsphere cores. This synthetic procedure is straightforward and inexpensive, and consequently can be readily adopted to produce larger quantities of the carbon@MoS_2 core-shell microspheres. After simple heat-treatment, the carbon@MoS_2 core-shell microspheres with outstanding structural features including the supportive nitrogen-doped carbon cores, the porous shells and the few-layered MoS_2 nanowalls with the enlarged interlayer distances can help solve the interrelated challenges of poor ionic and electronic transport and volume strain during cycles in the MoS_2 anodes. Therefore, these microspheres exhibit the good reversibility, the excellent capacity stability and the rate performance up to 2000 mA g^{-1}. Furthermore, the thin carbon coating on the carbon@MoS_2 core-shell microspheres could help to further preserve higher capacity and maintain higher electrochemical stability. A very high reversible capacity of 856 mAh g^{-1} is obtained after 100 cycles at 100 mA g^{-1}. In view of the excellent electrochemical performances and the facile and cost-effective synthesis, the carbon@metal sulphides core-shell microspheres on the basis of hierarchical nanoarchitectures might hold great promise to improve the electrochemical performances of the advanced Li-ion batteries.

Acknowledgements

This work was partly supported by China Postdoctoral Science Foundation (No.2014M560306), Grant from Science and Technology Commission of Shanghai Municipality (No. 15YF1402800) and Fundamental Research Funds for the Central Universities (No. 222201414033).

References

1 Y. Liang, R. Feng, S. Yang, H. Ma, J. Liang, J. Chen, *Adv. Mater.*, 2011, **23**, 640.
2 Y. Liu, L. Jiao, Q. Wu, J. Du, Y. Zhao, Y. Si, Y. Wang, H. Yuan, *J. Mater. Chem. A*, 2013, **1**, 5822.
3 X. Huang, Z. Zeng, H. Zhang, *Chem. Soc. Rev.*, 2013, **42**, 1934.
4 G. Huang, T. Chen, W. Chen, Z. Wang, K. Chang, L. Ma, F. Huang, D. Chen, J. Y. Lee *Small*, 2013, **9**, 3693.
5 J. Xiao, X. Wang, X. Yang, S. Xun, G. Liu, P. K. Koech, J. Liu, J. P. Lemmon, *Adv. Funct. Mater.*, 2011, **21**, 2840.
6 X. Zhao, C. Hu, M. Cao, *Chem. Asian J.*, 2013, **8**, 2701.
7 H. Wang, H. Feng, J. Li, *Small*, 2014, **10**, 2165.
8 Y. Jing, Z. Zhou, C. R. Cabrera, Z. Chen, *J. Mater. Chem. A*, 2014, **2**, 12104.
9 X. Fang, X. Yu, S. Liao, Y. Shi, Y. Hu, Z. Wang, G. D. Stucky, L. Chen, *Micropor. Mesopor. Mater.*, 2012, **151**, 418.
10 Y. Shi, Y. Wang, J. I. Wong, A. Y. S. Tan, C. L. Hsu, L. J. Li, Y. C. Lu, H. Y. Yang, *Sci. Rep.*, 2013, **3**, 2169.
11 H. Yu, C. Zhu, Y. Chen, C. Li, P. Gao, P. Yang, Q. Ouyang, *J. Mater. Chem. A*, 2014, **2**, 4551.
12 J. Xiao, D. Choi, L. Cosimbescu, P. Koech, J. Liu, J. P. Lemmon, *Chem. Mater.*, 2010, **22**, 4522.
13 G. Du, Z. Guo, S. Wang, R. Zeng, Z. Chen, H. Liu, *Chem. Commun.*, 2010, **46**, 1106.
14 K. Chang, W. Chen, L. Ma, H. Li, H. Li, F. Huang, Z. Xu, Q. Zhang, J. Y. Lee, *J. Mater. Chem.*, 2011, **21**, 6251.
15 C. Zhang, Z. Wang, Z. Guo, X. W. Lou, *ACS Appl. Mater. Interfaces*, 2012, **4**, 3765.
16 K. Bindumadhavan, S. K. Srivastava, S. Mahanty, *Chem. Commun.*, 2013, **49**, 1823.
17 S. Ding, J. S. Chen, X. W. Lou, *Chem. Eur. J.*, 2011, **17**, 13142.
18 X. Zhou, L. J. Wan, Y. G. Guo, *Nanoscale*, 2012, **4**, 5868.
19 K. Chang, W. Chen, *Chem. Commun.*, 2011, **47**, 4252.
20 K. Chang, D. Geng, X. Li, J. Yang, Y. Tang, M. Cai, R. Li, X. Sun, *Adv. Energy Mater.*, 2013, **23**, 839.
21 K. Chang, W. Chen, *J. Mater. Chem.*, 2011, **21**, 17175.
22 S. K. Das, R. Mallavajula, N. Jayaprakash, L. A. Archer, *J. Mater. Chem.*, 2012, **22**, 12988.
23 U. K. Sen, S. Mitra, *ACS Appl. Mater. Interfaces*, 2013, **5**, 1240.
24 H. Hwang, H. Kim, J. Cho, *Nano Lett.*, 2011, **11**, 4826.

25 C. Zhang, H. B. Wu, Z. Guo, X. W. Lou, *Electrochem. Commun.*, 2012, **20**, 7.
26 C. Feng, J. Ma, H. Li, R. Zeng, Z. Guo, H. Liu, *Mater. Res. Bull.*, 2009, **44**, 1811.
27 Y. Chen, B. Song, X. Tang, L. Lu, J. Xue, *Small*, 2014, **10**, 1536.
28 P. Sun, W. Zhang, X. Hu, L. Yuan, Y. Huang, *J.Mater. Chem.A*, 2014, **2**, 3498.
29 Y. Gong, S. Yang, L. Zhan, L. Ma, R. Vajtai, P. M. Ajayan, *Adv. Funct. Mater.*, 2014, **24**, 125.
30 H. Liu, D. Su, R. Zhou, B. Sun, G. Wang, S. Z. Qiao, *Adv. Energy Mater.*, 2012, **2**, 970.
31 L. Su, Y. Jing, Z. Zhou, *Nanoscale*, 2011, **3**, 3967.
32 L. Zhang, X. W. Lou, *Chem. Eur. J.*, 2014, **20**, 5219.
33 R. G. Chaudhuri, S. Paria, *Chem. Rev.*, 2012, **112**, 2373.
34 J. Besnardiere, X. Petrissans, C. Surcin, V. Buissette, T. LeMercier, M. Morcrette, D. Portehault, S. Cassaignon, *RSC Adv.*, 2014, **4**, 21208.
35 C. Avendaño, A. Briceño, F. J. Méndez, J. L. Brito, G. González, E. Cañizales, R. Atencio, P. Dieudonné, *Dalton Trans.*, 2013, **42**, 2822.
36 H. Zhou, S. Xu, H. Su, W. Mei, W. Qiao, L. Ling, D. Long, *Chem. Commun.*, 2013, **49**, 3763.
37 S. K. Park, S. H. Yu, S. Woo, J. Ha, J. Shin, Y. E. Sung, Y. Piao, *CrystEngComm*, 2012, **14**, 8323.
38 Q. Wang, J. Li, *J. Phys. Chem. C*, 2007, **111**, 1675.
39 Y. Jing, E. O. Ortiz-Quiles, C. R. Cabrera, Z. Chen, Z. Zhou, *Electrochim. Acta*, 2014, **147**, 392.
40 Y. Li, D. Wu, Z. Zhou, C. R. Cabrera, Z. Chen, *J. Phy. Chem. Lett.*, 2012, **3**, 2221.
41 M. Wang, G. Li, H. Xu, Y. Qian, J. Yang, *ACS Appl. Mater. Interfaces*, 2013, **5**, 1003.
42 Li. Yang, S. Wang, J. Mao, J. Deng, Q. Gao, Yi Tang, O. G. Schmidt, *Adv. Mater.*, 2013, **25**, 1180.
43 L.Su, Z. Zhou, X. Qin, Q. Tang, D. Wu, P. Shen, *Nano Energy*, 2013, **2**, 276.
44 L. Su, Y. Zhong, Z. Zhou. *J. Mater. Chem. A*, 2013, **1**, 15158.
45 Y. Zhong, M. Yang, X. Zhou, Y. Luo, J. Wei, Z. Zhou, *Adv. Mater.*, 2015, **27**, 806.
46 S. Ding, D. Zhang, J. S. Chen, X. W. Lou, *Nanoscale*, 2012, **4**, 95.
47 L. Yang, S. Wang, J. Mao, J. Deng, Q. Gao, Y. Tang, O. G. Schmidt, *Adv. Mater.*, 2013, **25**, 1180.